Supplementary Information

Materials and Methods:

Peptides, proteins, and nucleic acids sample preparation: The following peptide sequences were used in our study: RP_3 = $\{RRASL\}_3$[1]; SR_8: $\{SR\}_4$ENLYFQG$\{SR\}_4$. Peptides were custom synthesized (≥ 95% purity) by GenScript USA Inc. (NJ, USA) and used without any further purification. Codon optimized wild-type (WT) FUS was gene synthesized by GenScript and cloned into (cloning site: SspI-BamHI) pET His6 MBP N10 TEV LIC cloning vector (2C-T). The plasmid vector was a gift from Scott Gradia (Addgene plasmid # 29706). TEV-cleaved FUS contained three exogenous amino acids (SNI) at its N-termini. *E. Coli* cells (BL21(DE3)) were transformed with the plasmids containing WT FUS and its variants in respective cases. Transformed cells were induced with IPTG (0.5 mM final concentration) at OD = 0.6-0.8 and further grown for an additional 3-5 hrs at 30 ^oC. Protein extraction was performed using a microfluidizer in lysis buffer (50 mM Tris-HCl, 10 mM imidazole, 1 M KCl, pH 8.0) containing a protease inhibitor cocktail (Roche). Cell debris was removed by centrifugation. His-tag proteins were purified from the crude cell lysate using Ni-NTA agarose matrix (Qiagen Inc, Valencia, CA) by gravity-flow chromatography following the manufacturer's protocol with the following modifications: the wash buffer included 1.5 M KCl to disrupt nucleic acid binding to the recombinant protein[2,3], which was eluted with elution buffer containing 250 mM imidazole and 150 mM NaCl, followed by extensive dialysis to remove imidazole. Finally, His_6-MBP-N10 was removed by the action of TEV (GenScript USA Inc.) and the recombinant protein was purified by flowing the reaction mixture through Ni-NTA agarose matrix. The purity of the eluted protein samples was checked using A_{280}/A_{260} measurements (to rule out the presence of nucleic acids), SDS-PAGE and ESI-mass spectrometry (Scripps Center for Mass Spectrometry).

Polyuridylic acid (polyU; molecular weight = 600-1000 kDa) and polyadenylic acid (polyA; molecular weight = 100-500 kDa) were purchased from Sigma-Aldrich. Nuclease-free water was purchased from Santa Cruz Biotechnology Inc. RNA and DNA oligos, U_{40} and T_{40}, were purchased from Integrated DNA Technologies (IDT). The nucleic acid samples were prepared by dissolving them in nuclease-free water, followed by concentration measurements by absorbance at 260 nm using a NanoDrop 2000c UV-Vis spectrophotometer.

Fluorescence Labeling: The peptides were labeled at the N-terminal amine using the NHS-ester derivative of Alexa594 dye (Molecular Probes) following our previously published protocol[4]. The A313C variant of the C-terminal domain LCD of FUS (LCD-2; 174-526Δ422-523) was purified using an identical protocol as described above for the WT protein and fluorescently labeled with Alexa488 dye (C5-maleimide derivative, Molecular Probes) using Cys-maleimide chemistry as described in our earlier work[5]. The labeling efficiency for all samples was observed to be ≥ 90% (UV-Vis absorption measurements), and no additional attempt was made to purify them further, given that only labeled protein is observed in the experiments.

Sample preparation for phase separation measurements: All of the peptide samples were diluted from the stock solutions in phase separation buffer (PS buffer; 10 mM Tris-HCl, pH 7.9) containing 50 mM NaCl unless otherwise noted. The peptide stocks were made in nuclease-free water. For the salt titration experiments, variable [NaCl] were used ranging from 0 mM to 225 mM. The turbidity measurements at 350 nm were performed using a NanoDrop 2000c UV-Vis spectrophotometer at room temperature unless otherwise noted. Desired amounts of ssRNA or ssDNA were added to the peptide solutions from the stock in nuclease-free water with appropriate salt concentrations to achieve the desired peptide:RNA (wt/wt)

ratio. Each sample was incubated 30 seconds prior to turbidity measurements using a 1 mm optical path length. Phase diagrams were constructed by plotting absorbance at 350 nm (A_{350}) as a function of RNA:peptide or RNA:protein. Critical points (C_1 and C_2) were determined by the cutoff values of A_{350} where droplets were visible within 30 seconds of incubation under a light microscope using a 100x oil immersion objective. The boundary conditions (C_0) were determined by the peak value of A_{350} at the RNA-peptide or RNA-protein concentration plane.

For the microscopy experiments with FUS, the MBP-His_6 tag was digested using TEV *in situ* after the protein was exchanged to the PS buffer containing 150 mM NaCl. The maximum stock concentration of FUS used in our study was 30 µM, which remained clear at 30 ºC without any sign of phase separation. Complete digestion by the protease was ensured by SDS-PAGE analysis within 2 hours of incubation of the reaction mixture at 30 ºC. Turbidity measurements were performed at room temperature with 10 or 20 µM protein sample and increased concentrations of ssRNA as described for the peptide samples.

Confocal Fluorescence Microscopy: The fluorescence and DIC imaging were performed using a Zeiss LSM 780 laser scanning confocal microscope, equipped with a 63x oil immersion objective (Plan-Apochromat 63x/1.4 Oil DIC M27). Samples were prepared and imaged using Nunc Lab-Tek Chambered Coverglass (ThermoFisher Scientific Inc) at room temperature unless otherwise noted, with 0.2–1.0 µM labeled samples within the bulk of unlabeled materials. For RNA-induced reentrant phase transition, 2 µl RNA were injected into a 20 µl sample volume into the bulk phase while imaging was performed at the coverslip. Control experiments were also performed with injection of just buffer solutions without RNA of identical volume, which produced no effect. To evaluate RNA concentration dependence of the droplet dissolution kinetics as well as the temporal dynamics of the vacuoles, the amount of RNA injected into the solution was estimated from the respective phase diagrams (Fig. S9). For the RP_3/polyU system (Fig. 1a), the final polyU:peptide ratio that was probed by microscopy ranged from 2.5 to 10. For the FUS/polyU system, stable vacuoles were formed by the addition of RNA to the phase-separated FUS (10-30 µM) to a final ratio of 1:0.05 (FUS:RNA), while droplet dissolution was triggered by injecting RNA to a final ratio of 1:2.55 (FUS:RNA). For Alexa488-labeled samples, the excitation and emission wavelengths were 488 nm/503-549 nm, and for Alexa594-labeled samples, the excitation and emission wavelengths were 561 nm/602-632 nm. Fluorescence recovery after photobleaching (FRAP) experiments were performed using the same confocal setup. The samples were bleached using 10 iterative pulses of total time ~6.5 s utilizing 100% laser power. Analyses were performed using average fluorescence intensities from three regions of interrogation (ROI) corresponding to photobleaching, reference, and background. The images and videos were analyzed using Fiji software[6].

Electrophoretic Mobility Measurements: Electrophoretic mobility of the peptide samples was measured as a function of RNA concentration using a Dynamic Light Scattering (DLS) apparatus (ZetasizerNano ZS; Malvern Instruments Ltd) using the phase analysis light scattering technique, known as M3-PALS. 200 µM of RP_3 (0.3538 $mg.mL^{-1}$) or SR_8 (0.5644 $mg.mL^{-1}$) was titrated against polyU RNA from 1:0 to 1:10 ratio (wt/wt) in 10 mM Tris-HCl, pH 7.9 with a 2 minute incubation time for each measurement point. The zeta potential values were calculated from the mobility measurements using the Malvern Zetasizer software.

In Vitro Transcription by T7 RNA Polymerase: Transcription reactions were carried out with the MEGAshortscript high yield transcription kit (AM1354) from Ambion. RNA transcription reaction products are optimized for 20-500 nucleotides. Since molar yields in this range are independent of size,

larger products lead to a higher mass yield. To optimize the assembly and dissolution of droplets, a larger transcription product (400 nt) was chosen. This DNA template contains the T7 polymerase promoter minimum sequence (TAATACGACTCACTATAGGGAGA) followed by 400 nucleotides of the MBP sequence. This DNA template was made via PCR from the pET His6 MBP N10 TEV LIC cloning plasmid using the following primers (Fw: ATCCCGCGAAATTAATACGA; Rv: TAGCCACCAAAGCGGTCGT) and further isolated via Qiagen's gel extraction kit. In the presence of RP_3, transcription using the MEGAshortscript Kit was carried out to induce the assembly and disassembly of RNP granules. The transcription reaction was assembled containing a proprietary T7 10x reaction buffer, 10 mM of rNTPS (ATP, CTP, GTP, UTP), 50 nM of the 400 nt purified DNA template, 1 mM RP_3, and T7 polymerase to drive the reaction. A control without T7 polymerase was also carried out side-by-side. The transcription reaction was performed on a coverslip at 37ºC and visualized using the Zeiss LSM 780 laser scanning confocal microscope. Time points of RNP granules were taken every 15 minutes for the assembly, and every 5 minutes for disassembly. For disassembly, we first allowed RP_3 to form droplets with 1:2 (wt/wt) polyU before introducing the transcription mixture.

Supplementary Figures

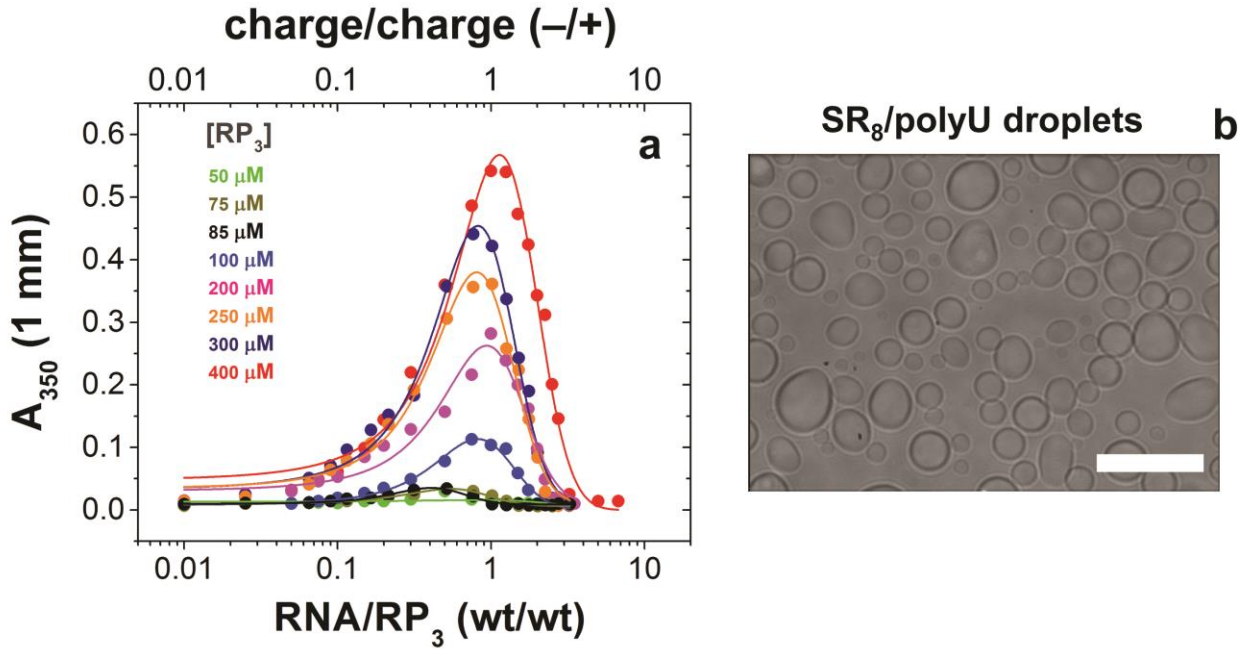

Figure-S1: (a) Phase boundary curves for RP_3/polyU system at different peptide concentrations, determined using solution turbidity measurements. The corresponding 2D contour plot is shown in Figure-1d in the main text. The charge ratios were calculated based on the average molecular weight of polyU RNA (600-1000 kDa; 2400-3100 bases) and exact molecular weight of the peptide (1769 Da; 6 Arg residues). **(b)** Light microscopy images of SR_8/polyU droplets at 50 mM NaCl with a peptide concentration of 200 µM, and 1:1 (wt/wt) polyU. Scale bar = 10 µm.

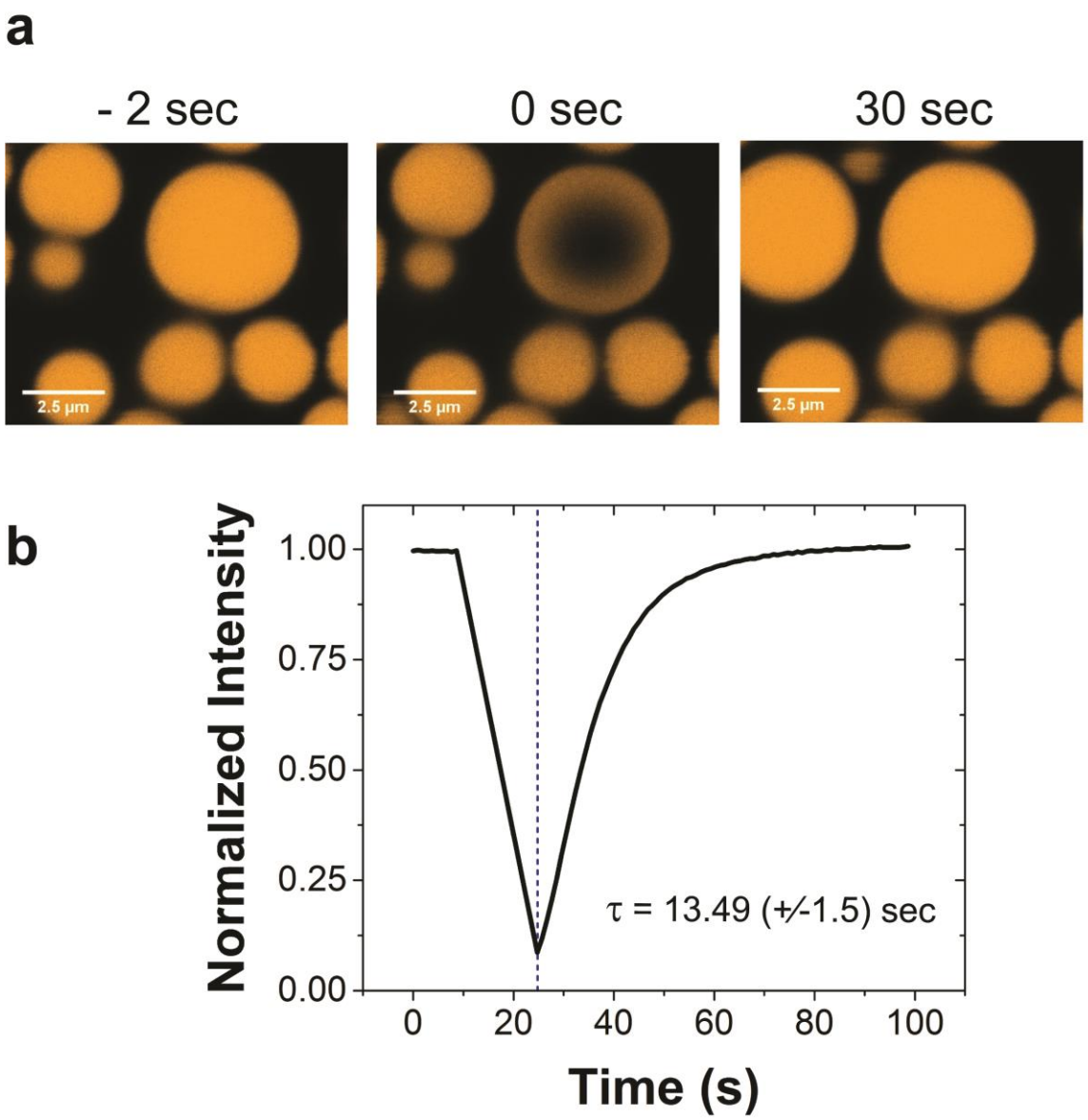

Figure-S2: Fluorescence recovery after photobleaching (FRAP) of RP_3/polyU droplets (200 µM peptide, and 1:1 (wt/wt) polyU). **(a)** Confocal fluorescence microscopy images of a pre-bleached (*right panel)*, bleached (*middle panel*), and recovered (*right panel*) RP_3/polyU droplet. (**b**) Kinetics of FRAP. The experimental data (black line) can be fitted to a single exponential model with a time constant (τ) of 13.5 s. The error bar is shown in the parenthesis. The dotted line refers to the 0 sec in *panel-a.*

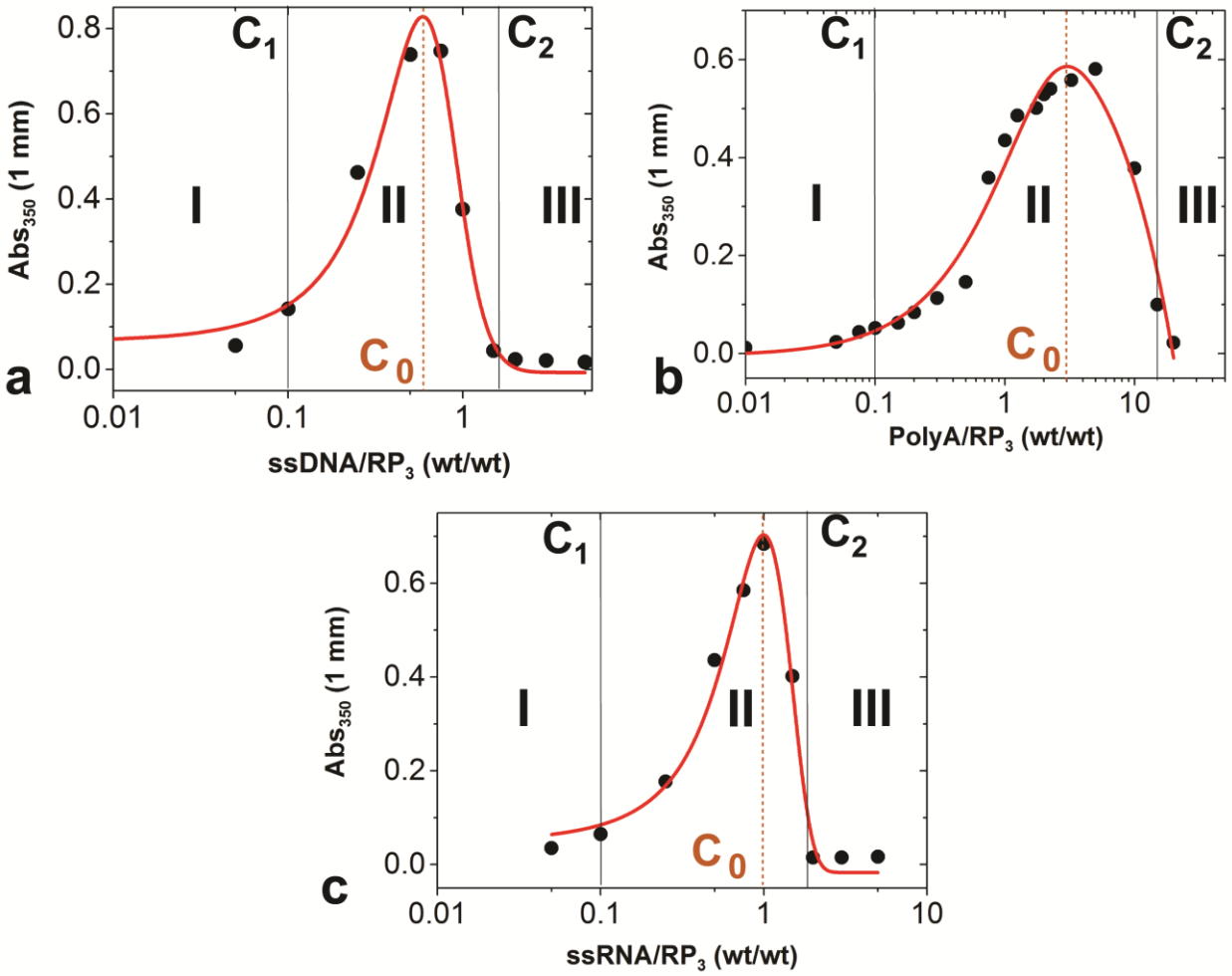

Figure-S3: (a), (b) and **(c)** Phase boundary curves for RP_3/T_{40}, RP_3/polyA and RP_3/U_{40} mixtures, respectively. These were determined by solution turbidity measurements. The critical concentrations (C_1 and C_2), boundary conditions (C_0), and three distinct regimes (I, II, and III) in the phase diagrams are highlighted. The peptide concentration was 200 µM in all cases.

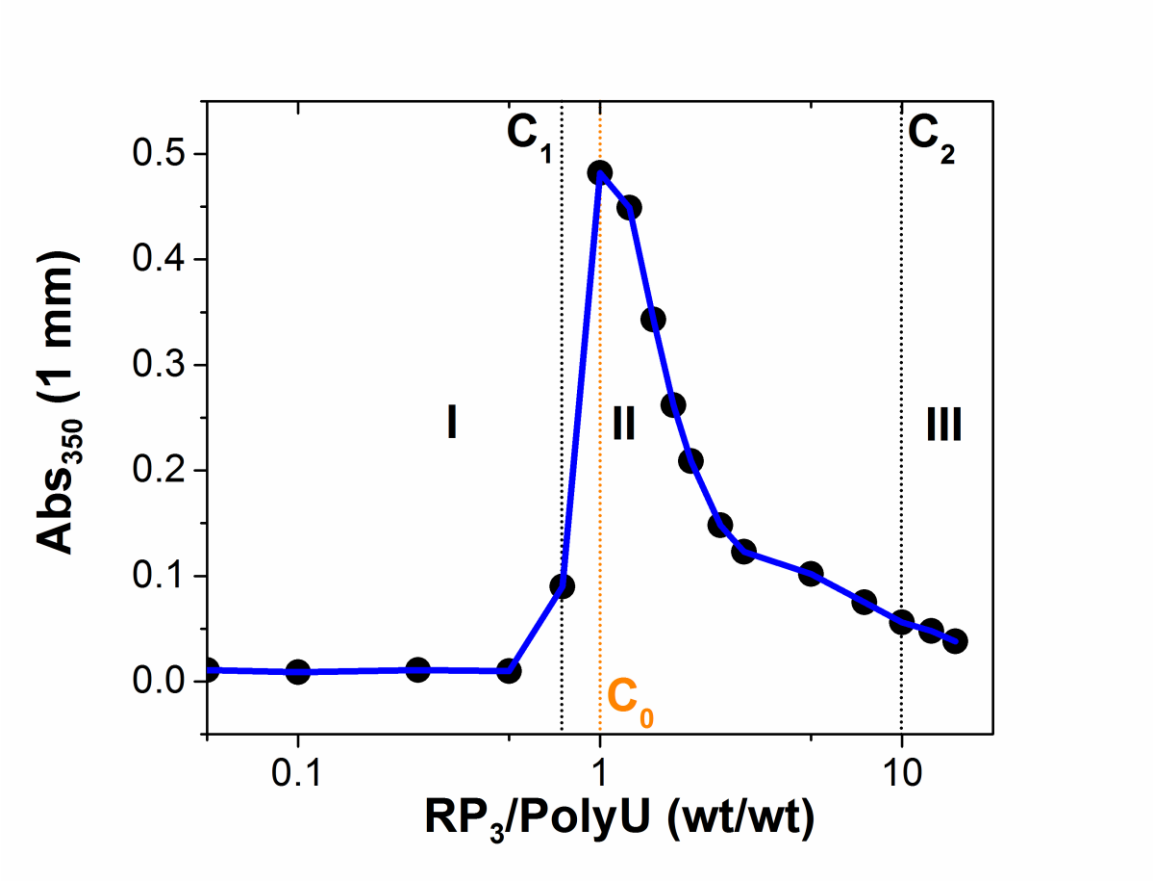

Figure-S4: RP_3/polyU phase boundary curve, obtained by a reverse titration. In this experiment, polyU concentration was kept fixed at 0.3538 mg/mL, while [RP_3] was monotonically varied. The critical concentrations (C_1 and C_2), the boundary condition (turbidity maximum; C_0), and three distinct regimes (I, II, and III) in the phase diagrams are highlighted.

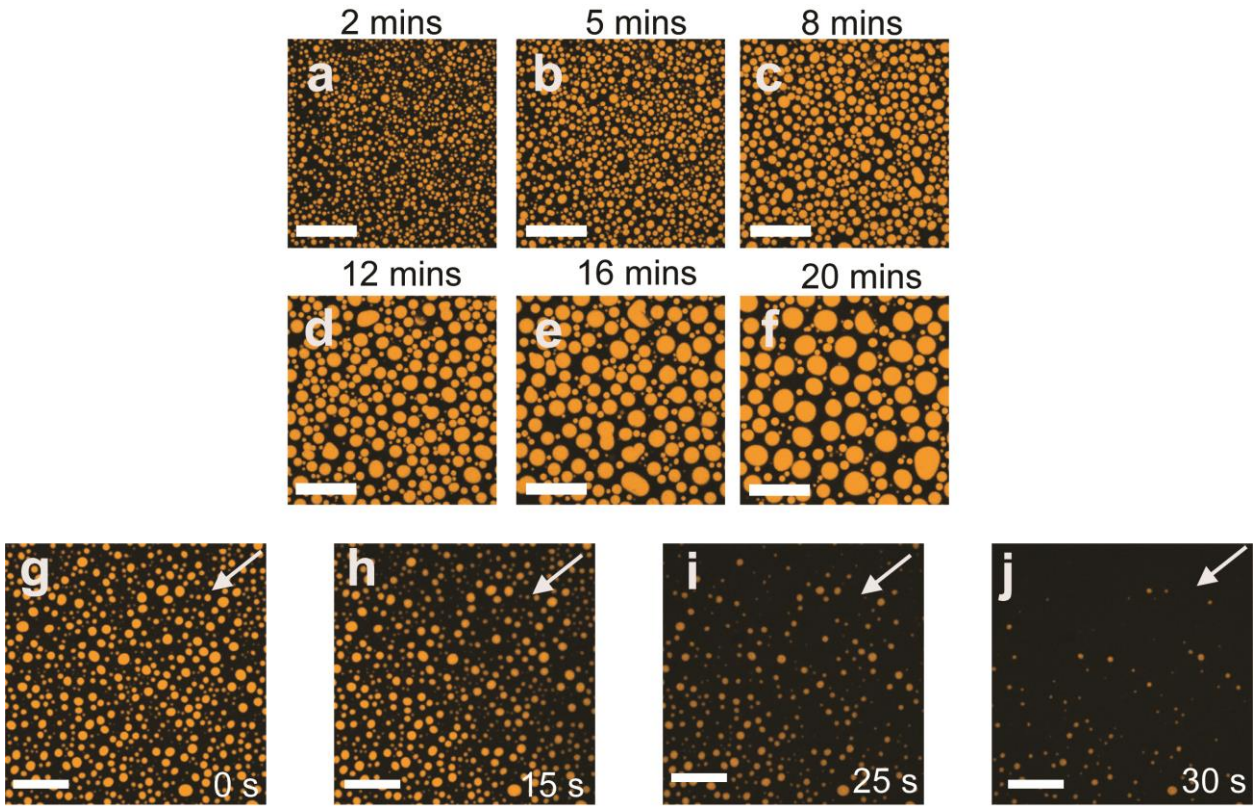

Figure-S5: (a)-(f) Temporal growth of the RP_3/polyU droplets on the microscope coverslip surface (500 µM peptide, and 1:1 (wt/wt) polyU) as observed using confocal fluorescence microscopy. Scale bar = 20 µm. **(g)-(j)** Directional dissolution of RP_3/polyU droplets by injection of 4 equivalent (wt/wt) RNA into a sample of RP_3/polyU droplets (200 µM peptide, and 1:1 wt/wt polyU). The direction of RNA influx has been indicated by a white arrow at the top right corner. Scale bar = 20 µm.

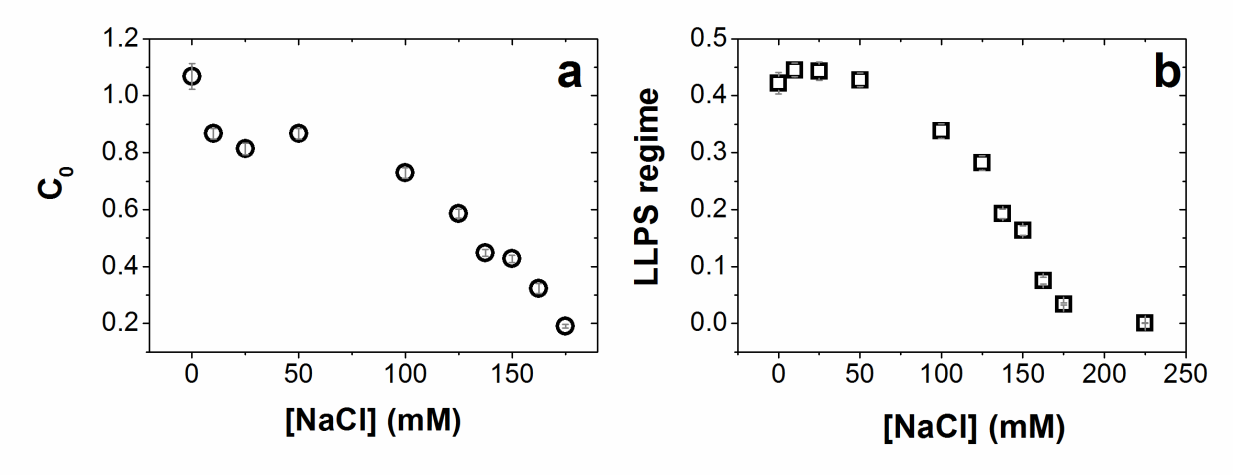

Figure-S6: (a) $\frac{[\text{RNA}]}{[\text{Peptide}]}$ corresponding to the solution turbidity maxima (C_0) for RP_3/polyU mixture as a function of [NaCl]. **(b)** The area under the LLPS regime (regime-II) plotted as a function of [NaCl]. The data corresponding to these plots is shown in Fig. 2a in the *main text.* Areas under the curve were determined by fitting the data from Fig. 2a in the *main text* using *Gaussmod* peak function in Origin 2016 NLS program. The observed trends can be explained by the theories of LLPS where electrostatic interactions play a dominant role (*i.e.*, complex coacervation). The theory of complex coacervation suggests that NaCl suppresses LLPS by lowering the free energy gain due to demixing[7,8], which is a result of weaker electrostatic interactions due to charge screening in the presence of salt. Furthermore, the higher the charge density and length (l) of a macromolecule, the lower the efficiency of screening by a monovalent ion[7]. Given the difference between the RP_3 (6 units of positive charge; l = 15 AA) and polyU (2400-3100 units of negative charge, l = 2400-3100 bases), NaCl is more effective in screening RP_3 than polyU, thereby decreasing the net positive charges (or +/– charge ratio) in the solution. Therefore, the boundary concentration, C_0, where LLPS is most favored, is progressively shifted towards lower values of $\frac{[\text{RNA}]}{[\text{Peptide}]}$ (or –/+ charge ratio) with increasing [NaCl] (also see Fig. 2a in the *main text*).

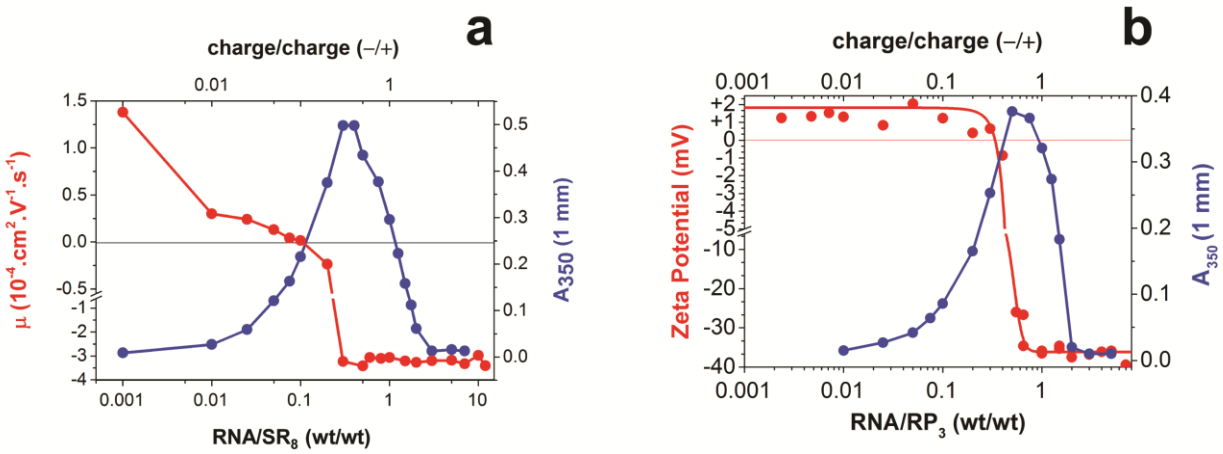

Figure-S7: (a) Overlay of electrophoretic mobility (red) and the solution turbidity (blue) for 200 μM SR_8 peptide in 10 mM Tris-HCl, pH 7.9, in presence of increasing [polyU]. **(b)** Overlay of zeta potential (red) and the solution turbidity (blue) for RP_3 peptide (200 μM) in 10 mM Tris-HCl, pH 7.9, in presence of increasing [polyU]. The zeta potential values were derived from electrophoretic mobility measurements, as shown in Fig. 2c in the *main text*. The charge ratios were calculated based on the average molecular weight of polyU RNA (600-1000 kDa; 2400-3100 bases) and exact molecular weights of the respective peptides (see *Materials and Methods*).

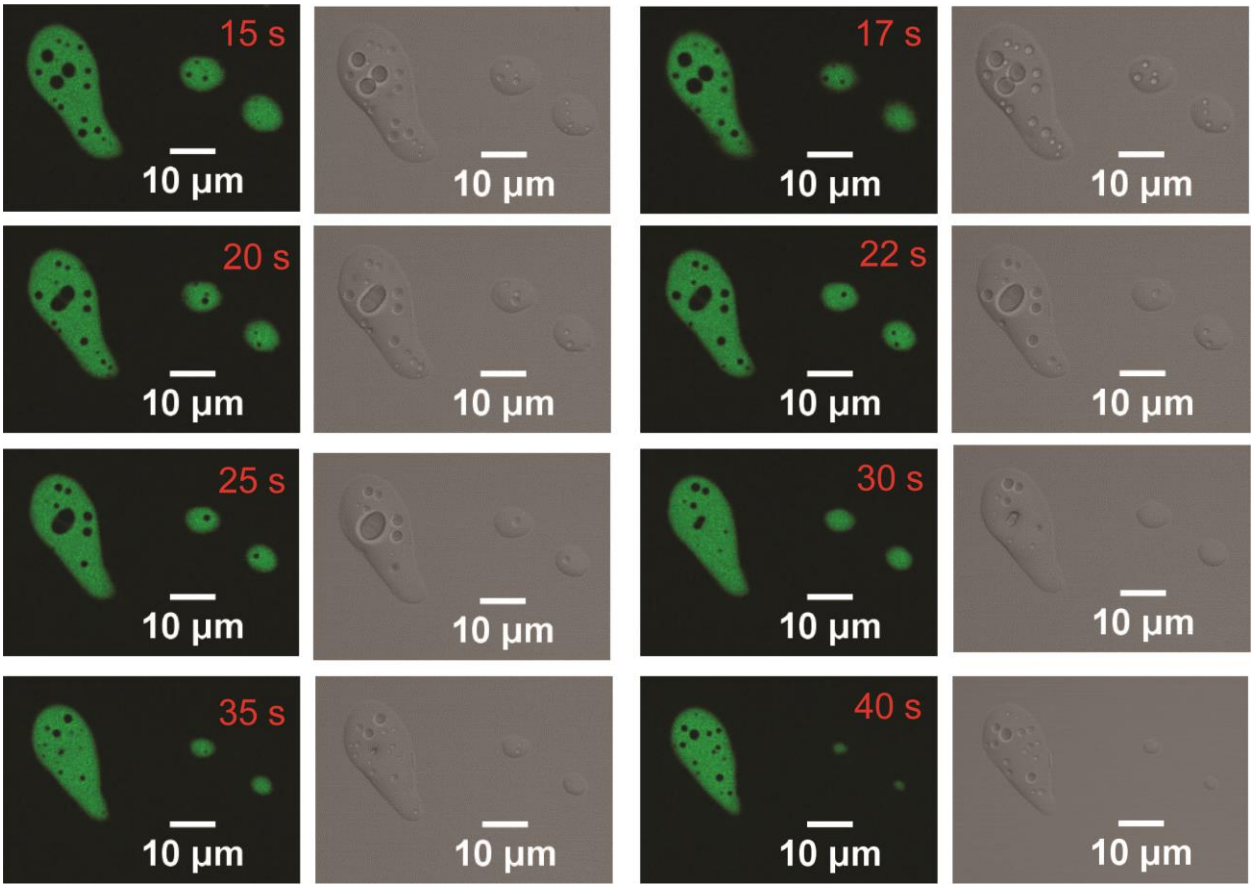

Figure-S8: Temporal dynamics of the vacuoles within RP_3/polyU droplets showing stochastic nucleation, fusion, and expulsion. Droplets were formed by mixing 200 µM peptide and 1:1 (wt/wt) polyU; while vacuole formation was triggered by jumping to 1:5 (wt/wt) polyU. The fluorescent droplets were imaged using the strategy of selective internalization of a free fluorophore, Alexa488. The corresponding video is shown in Movie-3.

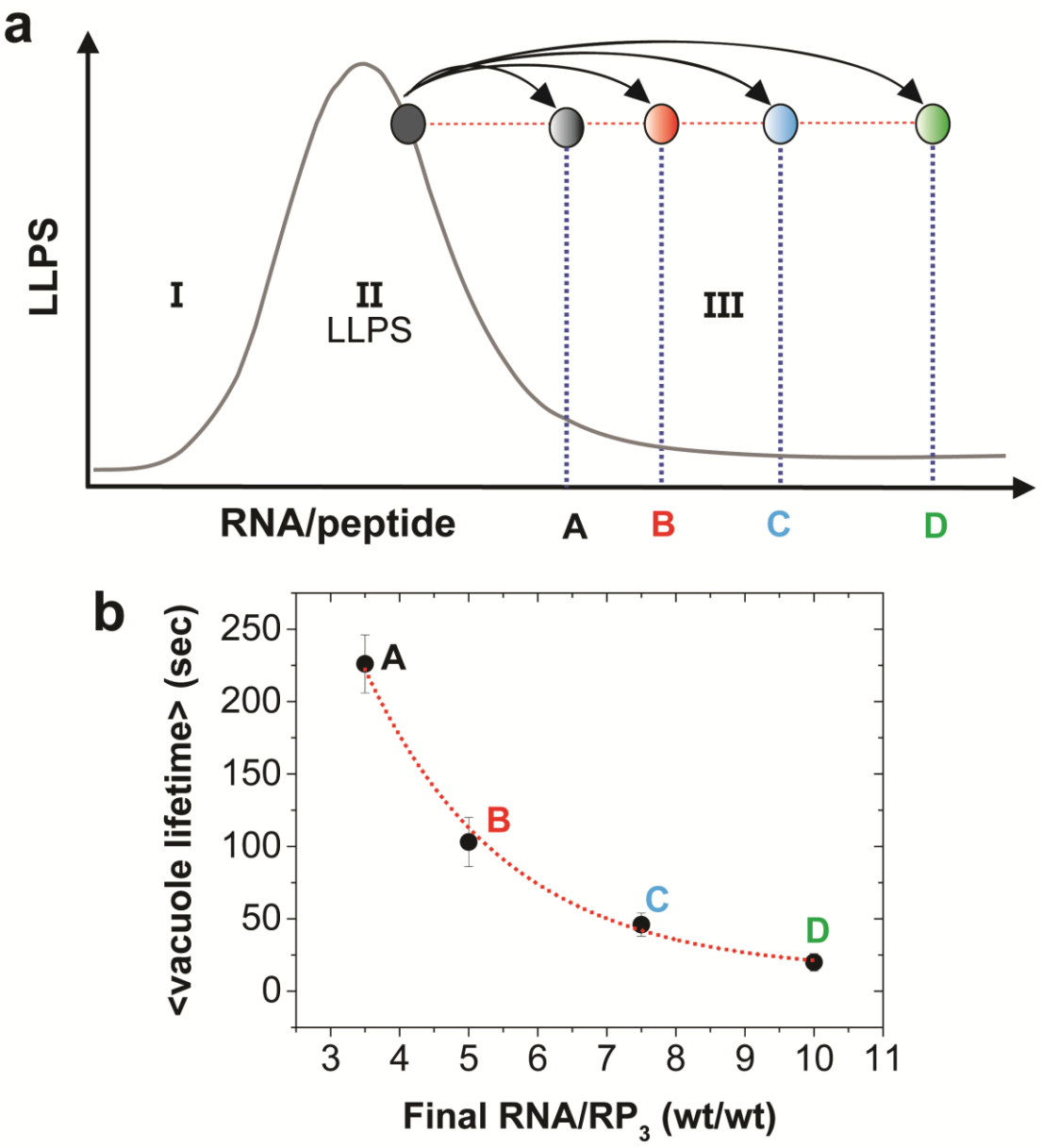

Figure-S9: (a) Illustration of RNA (polyU) concentration-jump at a fixed [peptide] from regime-II to various final compositions in regime-III for RP_3/polyU mixtures. The starting point is identical for all the measurements. (**b**) The average lifetime of the vacuoles (estimated using Fiji image/video processing software) plotted as a function of the final composition of the RP_3/polyU mixtures. The points appear to follow a single-exponential scaling law (red dotted line).

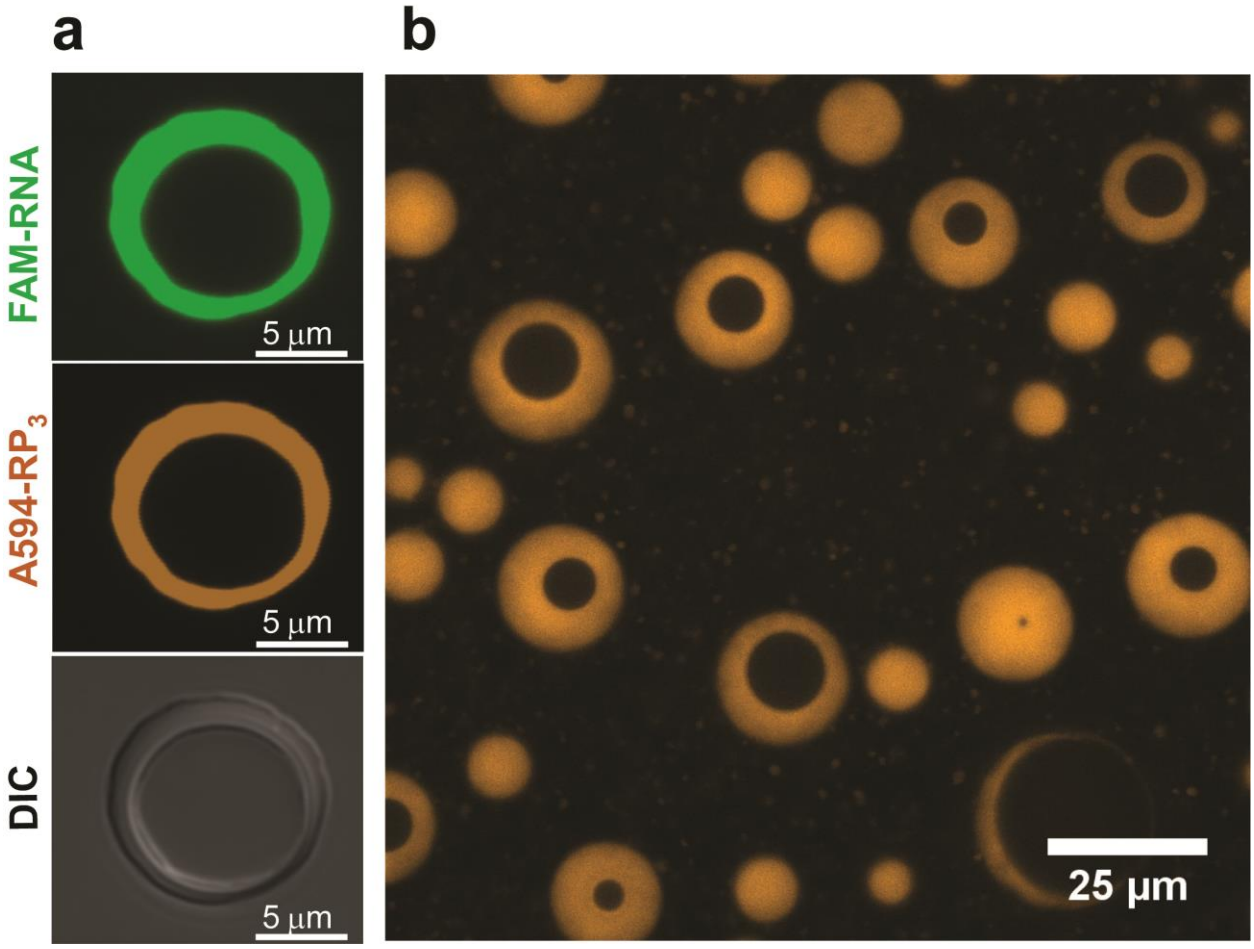

Figure-S10: (a) Vacuole within an RP_3/polyU droplet as imaged using a fluorescently labeled RNA probe (FAM-UGAAGGAC), RP_3 (Alexa594-RP_3) as well as DIC microscopy. **(b)** Persistence of vacuolated RP_3/polyU droplet morphology after 2hrs of their formation.

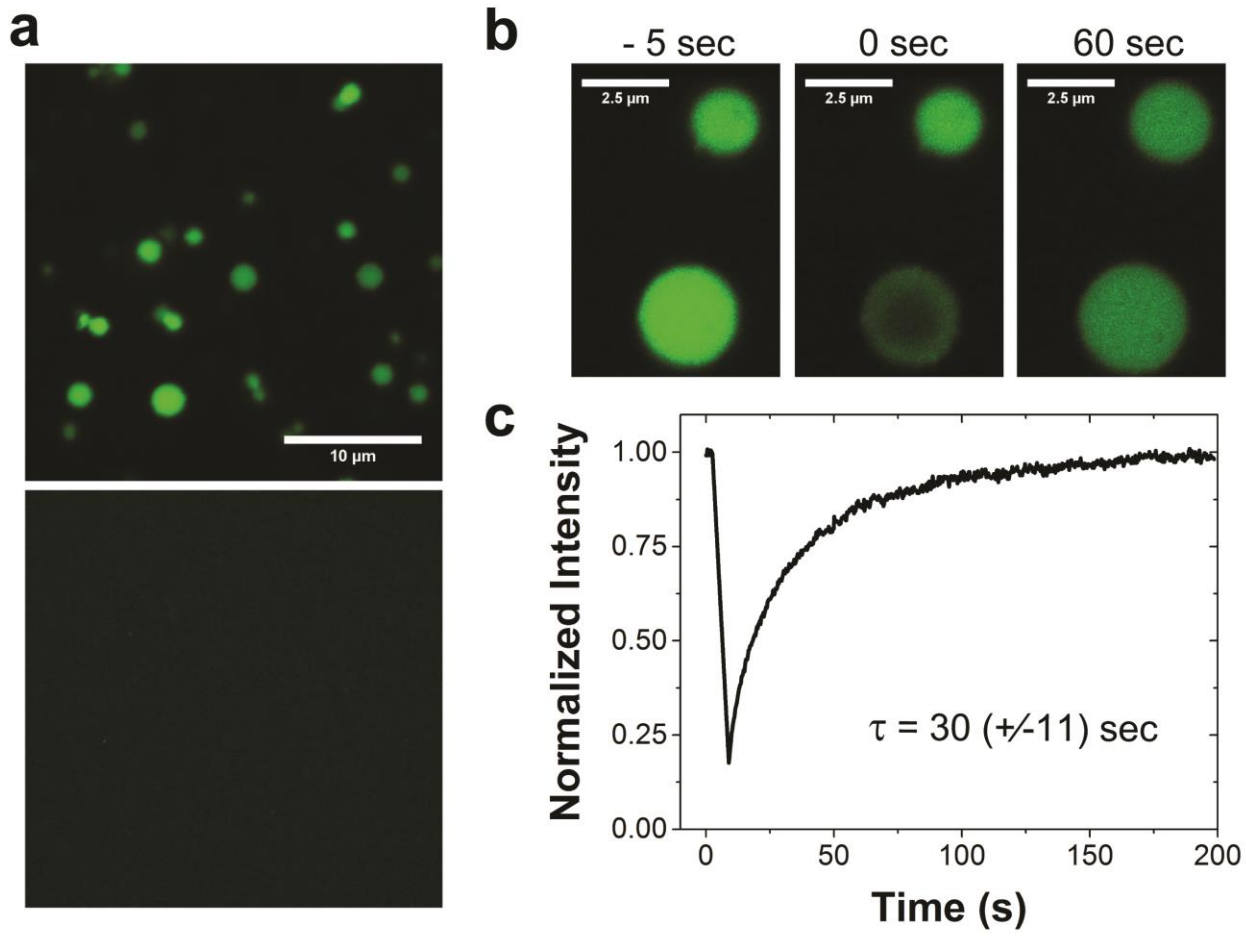

Figure-S11: (a) Liquid-liquid phase separation of FUS in presence of polyU (1:0.03; wt/wt) at room temperature (*top panel*), while FUS does not undergo homologous phase separation under the same condition (*bottom panel*; same scale bar as the top panel). **(b)** and **(c)** Fluorescence recovery after photobleaching (FRAP) of FUS/polyU droplets (10 µM FUS, and 1:0.03 (wt/wt) polyU) showing liquid-like behavior: Confocal fluorescence microscopy images of pre-bleached (*left panel*), bleached (*middle panel*), and recovered (*right panel*) droplets are shown in **(b)**. 0 sec reflects the time-point of bleaching. **(c)** Kinetics of FRAP. The experimental data (black line) can be fitted to a single exponential model with a time constant (τ) of ~ 30 s. The error bar is indicated in the parenthesis.

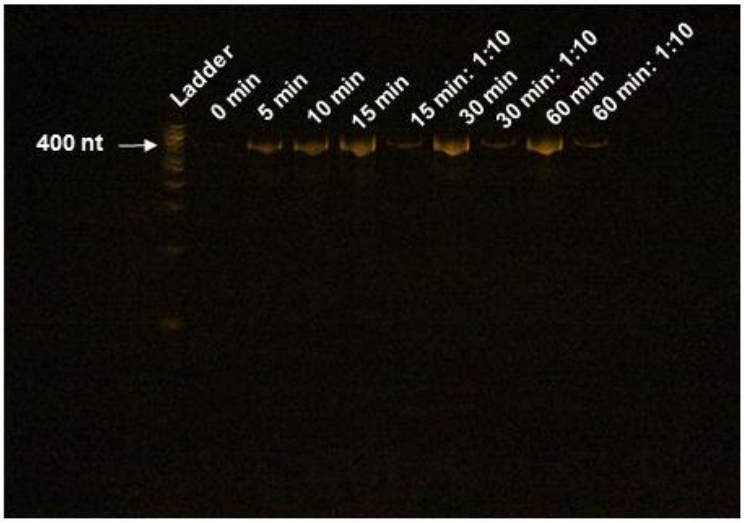

Figure-S12: 10% polyacrylamide, 8M urea/TBE gel showing RNA synthesis using T7 RNA polymerase kit from Ambion. The gel was stained using SYBR safe and visualized under blue light illumination. The time points are specified in the gel. The amount of the reaction mixture loaded into the gel is 0.1 µl from 20 µl reaction mixture (0.5%) except the following lanes: 15 min (1:10), 30 min (1:10) and 60 min (1:10), where the amount loaded was 0.05%.

Movie Legends

Movie-1: Temporal growth of the RP_3/polyU droplets showing fusion events. **Conditions:** 500 µM (0.87 mg/ml) unlabeled peptide containing 0.1% Alexa594-labeled peptide, and 1:0.5 (wt/wt) polyU. Speed = 14x.

Movie-2: Formation of RP_3/polyU droplets at randomly nucleated sites by the addition of 1 equivalent RNA (polyU; wt/wt). Peptide concentration = 200 µM (0.348 mg/ml). Speed = 7x.

Movie-3a: Temporal dynamics of vacuoles within RP_3/polyU droplets using confocal fluorescence microscopy. **Conditions:** droplets were initially prepared using 500 µM (0.87 mg/ml) unlabeled peptide containing 200 nM Alexa488 free dye, and 1:1 (wt/wt) polyU, followed by addition of 4 equivalent (wt/wt) of polyU. Speed = 7x.

Movie-3b: Temporal dynamics of vacuoles within RP_3/polyU droplets using DIC microscopy. **Conditions:** droplets were initially prepared by mixing 500 µM (0.87 mg/ml) unlabeled peptide with 1:1 (wt/wt) polyU, followed by addition of 4 equivalent (wt/wt) of polyU. Speed = 7x.

Movie-4a: Dynamics of RP_3/polyU droplets during RNA-mediated mixing phase transition using confocal fluorescence microscopy. **Conditions:** droplets were prepared using 2 mM unlabeled peptide containing 500 nM Alexa594-labeled peptide, and 1:0.5 (wt/wt) polyU, and allowed them to grow for 30 mins. The vacuole formation was triggered subsequently by jumping to 1.25 equivalent (wt/wt) of polyU. Speed = 28x.

Movie-4b: Dynamics of RP_3/polyU droplets during RNA-mediated mixing phase transition using DIC microscopy. **Conditions:** droplets were prepared by mixing 2 mM unlabeled peptide and 1:0.5 (wt/wt) polyU, and allowed them to grow for 30 mins. The vacuole formation was triggered subsequently by jumping to 1.25x equivalent (wt/wt) of polyU. Speed = 28x.

Movie-5: Formation and dissolution of RP_3/polyU droplets by the addition of RNA (polyU). Peptide concentration = 200 µM. Speed = 7x.

Movie-6a: Dynamics of FUS/polyU droplets during reentrant phase transition using confocal fluorescence microscopy. **Conditions:** droplets were initially prepared using 10 µM unlabeled protein containing 200 nM Alexa488-labeled FUS (LCD-2), and 1:0.03 (wt/wt) polyU. The vacuole formation and droplet dissolution were subsequently triggered by the addition of 2.5 equivalent (wt/wt) of polyU. Speed = 7x.

Movie-6b-i: dynamics of vacuoles within FUS/polyU droplets (with lifetime $\geq$ 60 s) using confocal fluorescence microscopy. **Conditions:** FUS droplets were initially prepared using 10 µM unlabeled protein containing 200 nM Alexa488-labeled FUS (LCD-2), and 1:0.025 (wt/wt) polyU, followed by jumping to 1:0.05 (wt/wt) of polyU. **Movie-4b-ii:** dynamics of vacuoles within FUS/polyU droplets (with lifetime $\geq$ 60 s) using DIC microscopy. **Conditions:** Same as Movie-6b-i.

SI Note-1

Although mean-field approaches based on linear Debye-Hückel or nonlinear Poisson-Boltzmann approximations provide fundamental frameworks to model charge screening in chemical and biological systems[9], they fail to explain reentrant phase transitions driven by strong electrostatic correlations[8]. This is well exemplified by the study of reentrant DNA condensation by multivalent cations and basic proteins such as histones[10]. Over the last two decades, post-mean-field theories have been developed to account for the reentrant condensation of DNA[10]. One of the widely applied theories predicts charge inversion as the underlying mechanism of reversible DNA condensation, which has also been experimentally validated[11].

The charge inversion model predicts a continuous reversible condensation transition for a charged multivalent macroion, induced by an oppositely charged multivalent counterion. In the case of a basic polypeptide (such as RP_3 peptide used in our experiments) and an acidic multivalent counterion (RNA in our case), the phase behavior due to electrostatic interactions is driven by the effective potential $\varphi = (kT/Z_{+/-}e)\ \ln(C/C_0)$[8]. Here Z_+ and Z_- represent the valency of the polypeptide and the RNA, respectively. The expression of φ suggests that the maximum gain in free energy due to demixing peaks at $C = C_0$, which is the charge inversion concentration. Furthermore, it predicts a non-monotonic (parabolic) shape of the phase boundary curve (y) that satisfies the following relation[8]:

$$y = 1 - a\left(\frac{n}{Z^2}\right) ln^2(C_0/C) \qquad (1)$$

Where the parameter *a* is given by

$$a = \left(\frac{kT}{4\xi\varepsilon}\right) ln(1 + r_s/b)$$

Here, ε is the energy of interaction per unit of positive charge in the units of thermal energy (kT), ξ is conventional Manning's parameter (~0.7 nm in the present case), r_s is the Debye's screening length, and b is the radius of the cylinder that represents an approximated geometry of the polypeptide chain. Without the exact knowledge of *a*, we can still use equation-1 to model the general shape of the phase boundary curve, and its dependence on $\left(\frac{n}{Z}\right)$. This is shown in Fig. S13:

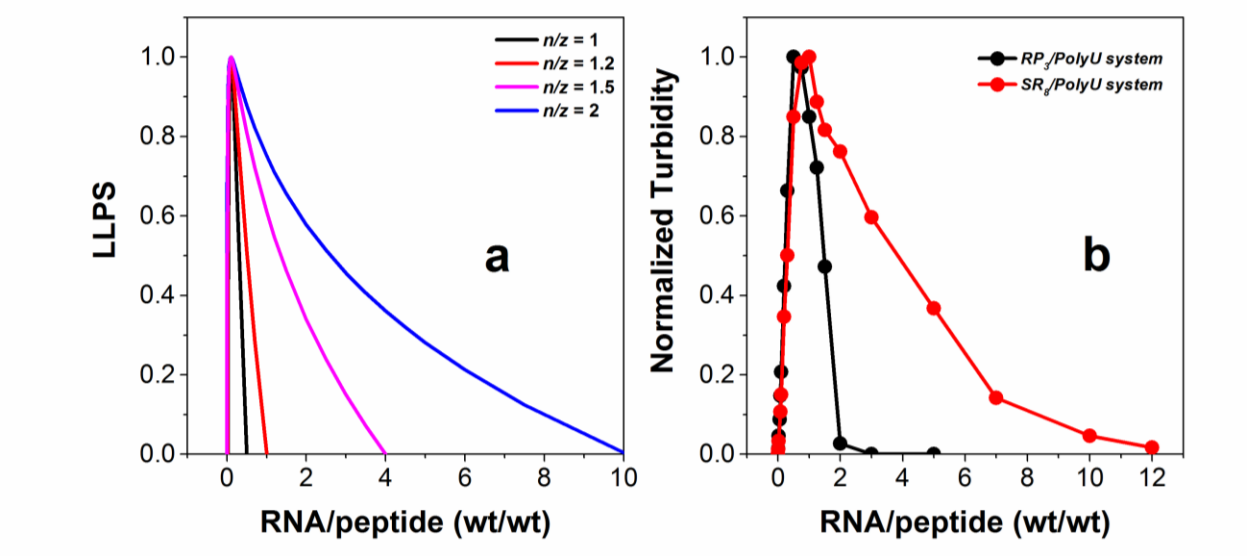

Figure-S13: (**a**) Numerical calculation based on equation-1 predicts a non-monotonic shape of the phase boundary curve. Also shown is the predicted effect of variation of *n/z* on the phase boundary curves. Our experimental data for RP_3/polyU and SR_8/polyU systems are shown in (**b**).

Overall, our phase boundary curves qualitatively agree with the charge inversion model. We have experimentally tested for charge inversion that may accompany the reentrant phase behavior of our systems. The experimental demonstration of charge inversion is presented in Fig. 2 of the *main text* and Fig. S7 in the SI.

SI Note-2

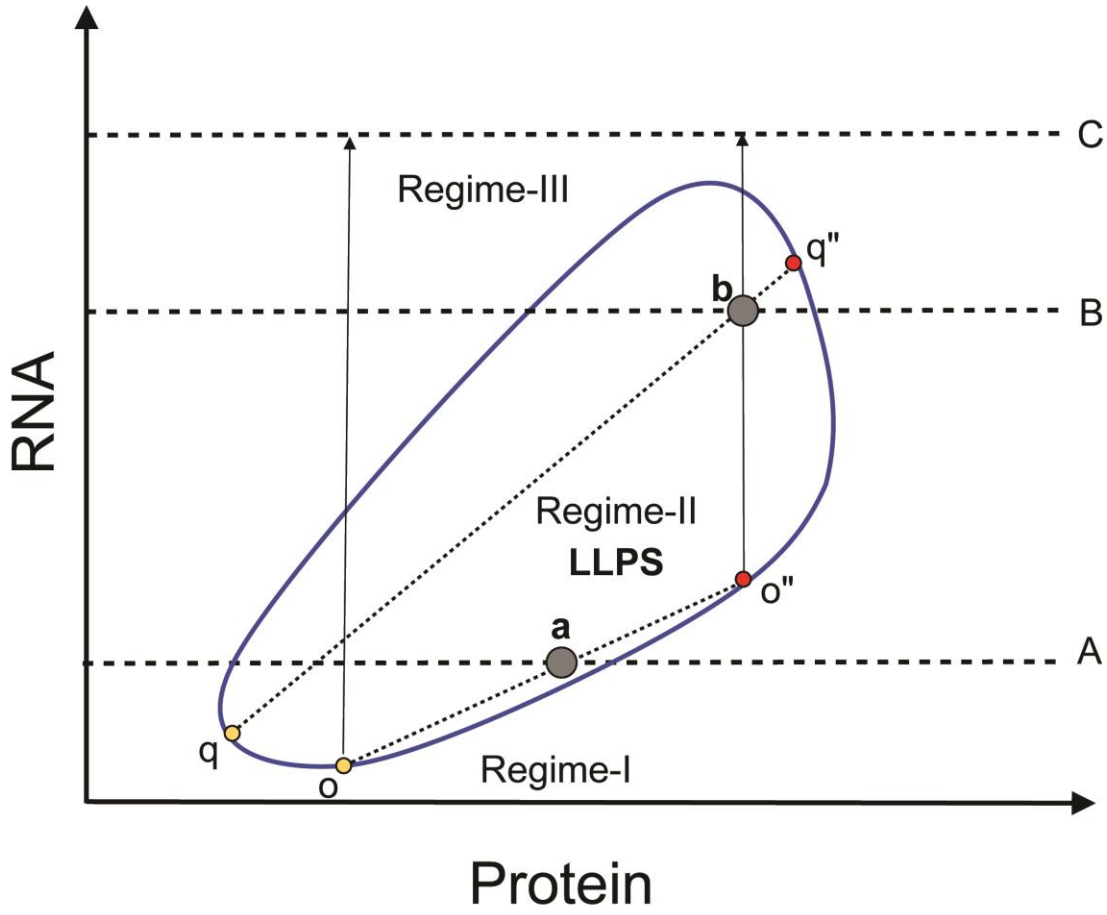

Figure-S14: Based on the recent theoretical predictions[12], we assume a closed-loop phase diagram in the present system of interest. At any given point of the RNA-protein concentration plane within the LLPS regime (regime-II), such as *point-a*, the equilibrium composition of the coexisting phases (dilute phase-*yellow point*; dense phase-*red point*) are given by the corresponding tie-line (oo" line). Now, a jump in RNA concentration from A to C will take the system out of the LLPS regime. We note that the regime-I and regime-III represent single phase regions in the phase diagram with one homogeneous phase. Therefore, the dense phase within regime-II will undergo a phase transition during this jump. If a nucleation-dependent-growth mechanism is followed, it is expected that a droplet morphology will be observed within the dense phase matrix similar to the forward phase transition when RNA was added to the RP_3 solution[13], and droplets of the dense phase were observed to be nucleated at random sites (Movie-2) within the bulk dilute phase. However, the system will be unstable due to the crossover condition, leading to an overall rapid dissolution dynamics of the vacuolated dense phase droplets. This condition is reminiscent of what is shown in Movie-3. In the case of an intermediate jump in RNA concentration (from concentration A to B), the dense phase still does not completely crossover (*point-b*), but must adjust to the new equilibrium compositions given by the tie-line under that condition (qq" line). Therefore, similar to the first condition,

the dense phase droplets will undergo further phase separation leading to the formation of droplets of dilute phases (vacuoles) within the dense phase matrix. In this case, however, the vacuoles will be more stable due to the boundary conditions of LLPS regime. This condition is reminiscent of what is shown in Movie-4.

Supplementary References

1 Aumiller, W. M., Jr. & Keating, C. D. Phosphorylation-mediated RNA/peptide complex coacervation as a model for intracellular liquid organelles. *Nat Chem* **8**, 129-137, doi:10.1038/nchem.2414 (2016).

2 Wang, X., Schwartz, J. C. & Cech, T. R. Nucleic acid-binding specificity of human FUS protein. *Nucleic Acids Research*, doi:10.1093/nar/gkv679 (2015).

3 Schwartz, J. C., Wang, X., Podell, E. R. & Cech, T. R. RNA seeds higher-order assembly of FUS protein. *Cell Rep* **5**, 918-925, doi:10.1016/j.celrep.2013.11.017 (2013).

4 Polinkovsky, M. E. *et al.* Ultrafast cooling reveals microsecond-scale biomolecular dynamics. *Nat Commun* **5**, 5737, doi:10.1038/ncomms6737 (2014).

5 Banerjee, P. R., Moosa, M. M. & Deniz, A. A. Two-Dimensional Crowding Uncovers a Hidden Conformation of alpha-Synuclein. *Angew Chem Int Ed Engl* **55**, 12789-12792, doi:10.1002/anie.201606963 (2016).

6 Schindelin, J. *et al.* Fiji: an open-source platform for biological-image analysis. *Nat Methods* **9**, 676-682, doi:10.1038/nmeth.2019 (2012).

7 Overbeek, J. T. & Voorn, M. J. Phase separation in polyelectrolyte solutions; theory of complex coacervation. *J Cell Physiol Suppl* **49**, 7-22; discussion, 22-26 (1957).

8 Nguyen, T. T., Rouzina, I. & Shklovskii, B. I. Reentrant condensation of DNA induced by multivalent counterions. *The Journal of chemical physics* **112**, 2562-2568, doi:10.1063/1.480819 (2000).

9 Grosberg, A. Y., Nguyen, T. T. & Shklovskii, B. I. Colloquium. *Reviews of Modern Physics* **74**, 329-345 (2002).

10 Teif, V. B. & Bohinc, K. Condensed DNA: condensing the concepts. *Progress in biophysics and molecular biology* **105**, 208-222, doi:10.1016/j.pbiomolbio.2010.07.002 (2011).

11 Besteman, K., Van Eijk, K. & Lemay, S. G. Charge inversion accompanies DNA condensation by multivalent ions. *Nat Phys* **3**, 641-644, doi:10.1038/nphys697.

12 Roosen-Runge, F., Zhang, F., Schreiber, F. & Roth, R. Ion-activated attractive patches as a mechanism for controlled protein interactions. *Sci Rep* **4**, 7016, doi:10.1038/srep07016 (2014).

13 Cheng, S. Z. D. in *Phase Transitions in Polymers* 61-76 (Elsevier, 2008).